

Original paper

Complementing knowledge about rare sulphates loncreekite, $\text{NH}_4\text{Fe}^{3+}(\text{SO}_4)_2 \cdot 12 \text{H}_2\text{O}$ and sabieite, $\text{NH}_4\text{Fe}^{3+}(\text{SO}_4)_2$: chemical composition, XRD and RAMAN spectroscopy (Libušín near Kladno, the Czech Republic)

Vladimír ŽÁČEK^{1*}, Radek ŠKODA¹, František LAUFEK¹, Filip KOŠEK², Jan JEHLIČKA²¹ Czech Geological Survey, Klárov 3, 118 21 Prague 1, Czech Republic; vladimir.zacek@geology.cz² Institute of Geochemistry, Mineralogy and Mineral Resources, Faculty of Science, Charles University, Albertov 6, 128 43, Prague 2, Czech Republic

* Corresponding author



Loncreekite and sabieite, hydrous and anhydrous ferric ammonium sulphates, were identified among the products of a long-lasting subsurface fire in the waste heap of the Schoeller coal mine in Libušín near Kladno, Central Bohemia, Czech Republic. No monomineralic fractions could be extracted as the minerals occur in a fine-grained aggregate with minor ferroan boussingaultite, tschermigite, and traces of efremovite. Powder X-ray diffraction, electron-microprobe analysis and Raman spectroscopy were used to identify the mineral phases in the mixture.

The empirical formula of loncreekite is $[(\text{NH}_4)_{0.98}\text{K}_{0.02}]_{\Sigma 1.00}(\text{Fe}_{0.70}\text{Al}_{0.24}\text{Mg}_{0.02})_{\Sigma 0.96}(\text{SO}_4)_{2.05} \cdot 12 \text{H}_2\text{O}$, and the calculated unit-cell ($P\bar{a}3$) parameter $a = 12.2442(2) \text{ \AA}$, with a cell volume of $V = 1835.68(9) \text{ \AA}^3$.

The composition of sabieite corresponds to the formula $[(\text{NH}_4)_{0.98}\text{K}_{0.02}]_{\Sigma 1.00}(\text{Fe}_{0.70}\text{Al}_{0.24}\text{Mg}_{0.02})_{\Sigma 0.96}(\text{SO}_4)_{2.05}$, and the calculated unit-cell parameters ($P3_21$) are $a = 4.826(1) \text{ \AA}$, $c = 8.283(2) \text{ \AA}$, $V = 167.10(8) \text{ \AA}^3$, assuming that only the 1T polytype is present. Raman spectroscopy was conducted on both minerals, giving strong Raman bands at 1037 cm^{-1} (ν_1), 1272 cm^{-1} (ν_3), 462 cm^{-1} (ν_2), 643 cm^{-1} (ν_4), 313 cm^{-1} ($M\text{-O}$ vibration) for sabieite; and at 991 cm^{-1} (ν_1), 1132 and 1104 cm^{-1} (ν_3), 461 and 443 cm^{-1} (ν_2), and 616 cm^{-1} (ν_4) for loncreekite (where ν_1 and ν_3 are stretching modes of the (SO_4) -group and ν_2 and ν_4 are bending modes). The sabieite most probably formed by *in situ* decomposition of the siderite-bearing sedimentary rock at $\sim 115\text{--}350 \text{ }^\circ\text{C}$. The loncreekite originated through hydration of the sabieite when the sample was stored at ambient temperature. Empirical formulae of associated ferroan boussingaultite and tschermigite are also given, respectively, as $(\text{NH}_4)_2(\text{Mg}_{0.62}\text{Fe}_{0.36}\text{Mn}_{0.06})_{\Sigma 1.04}(\text{SO}_4)_{1.97} \cdot 6 \text{H}_2\text{O}$ and $[(\text{NH}_4)_{0.98}\text{K}_{0.02}]_{\Sigma 1.00}(\text{Al}_{0.97}\text{Fe}_{0.06})_{\Sigma 1.03}(\text{SO}_4)_{2.97} \cdot 12 \text{H}_2\text{O}$.

Keywords: sabieite, loncreekite, Kladno, burning heaps, electron microprobe, Raman spectroscopy

Received: 29 November 2018; **accepted:** 21 May 2019; **handling editor:** J. Sejkora

1. Introduction

Sulphates are minerals that are commonly present in volcanic hydrothermal systems (e.g. Stoiber and Rose 1974), burning coal seams and coal mines waste heaps (e.g. Stracher et al. 2015) and as post-mining alteration products (e.g. Witzke and Rüger 1998). In all of these settings, the composition of sulphates reflects the peculiarities of mineral-forming environments. This has implications not only for the terrestrial, but can also for the planetary research, most notably the investigation of sulphate-bearing strata on Mars (e.g. Gendrin et al. 2005). Sulphates frequently occur as complex mixtures and their diversity is frequently multiplied by several stages of hydration (Culka et al. 2014). Reliable identification of separate compounds in such complex mixtures requires the application of several analytical methods. This is the case also for loncreekite and sabieite, two sulphates that compositionally differ only in their water content.

Loncreekite, cubic $(\text{NH}_4)\text{Fe}^{3+}(\text{SO}_4)_2 \cdot 12 \text{H}_2\text{O}$ – natural ammonium iron alum – and sabieite, trigonal $(\text{NH}_4)\text{Fe}^{3+}(\text{SO}_4)_2$, are rare ammonium-bearing sulphates found in several places around the World. The type locality of both minerals, and also of clairite $(\text{NH}_4)\text{Fe}^{3+}(\text{SO}_4)_2(\text{OH})_3 \cdot 3 \text{H}_2\text{O}$, is the Lone Creek Falls cave, near Sabie, in eastern Transvaal, South Africa (Martini 1984). The minerals were found to form together with other sulphates at an ambient temperature from seepage water that oxidized pyrite in the breccia above the cave and then interacted with ammonia from decaying excreta of rock hyrax (dassie, *Procapra capensis*). The sabieite was reportedly derived from the dehydration of loncreekite. The aluminium analogue of loncreekite is tschermigite $(\text{NH}_4)\text{Al}(\text{SO}_4)_2 \cdot 12 \text{H}_2\text{O}$, natural ammonium aluminium alum.

Loncreekite from the type locality has the empirical formula $(\text{NH}_4)_{0.99}[\text{Fe}^{3+}_{0.79}\text{Al}_{0.16}]_{\Sigma 0.95}(\text{SO}_4)_{2.12} \cdot 12.25 \text{H}_2\text{O}$, unit-cell parameter of $a = 13.302 \text{ \AA}$, $Z = 4$, space group $P\bar{a}3$, and calculated density of 1.69 g/cm^3 (Martini 1984).

Frost and Klopogge (2001) reported Raman bands of loncreekite at 307, 435, 463, 525, 615, 636, 701, 991, 1099, 1108, and 1134 cm^{-1} . Loncreekite has also been reported from the shale fire in Huron County, near the village of Milan, Ohio (Carlson 2010), from unspecified caves in Venezuela (Mindat 2019) and without detailed data from the Copiapó Province in Chile, the Pésc-Vasas mine in southern Hungary (Szakáll and Kristály 2008) and from the Humboldt Co., Nevada (Mindat 2018a).

The formula of sabieite is $\text{NH}_4\text{Fe}^{3+}(\text{SO}_4)_2$, the mineral is isostructural with godovikovite and possesses a glaserite-(aphthitalite-) type structure with $P3_21$ symmetry and unit-cell parameters of $a = 4.822$ and $c = 8.1696$ Å, and $Z = 1$ (PDF-2 record No. 24-44). Electron-microprobe analyses (EMPA) of the holotype mineral provided the empirical formula $[(\text{NH}_4)_{0.83}\text{K}_{0.04}]_{\Sigma 0.87}(\text{Fe}_{0.94}\text{Al}_{0.04})_{\Sigma 0.98}(\text{SO}_4)_{2.03}$ (Martini 1984). The Raman spectra of natural sabieite from burning heaps in Ostrava, Czech Republic were reported by Košek et al. (2017) (with bands at 183 m, 315 s, 464 m, 603 m, 646 m, 1041 vs, 1276 vw cm^{-1}). Sabieite was later well characterized based on material from the natural Huron oil-shale fire (Kampf et al. 2014). The mineral formed tiny brittle colourless to pink and yellow hexagonal tablets with perfect cleavage on $\{001\}$, and a measured density of 2.65(2) g/cm^3 . The mineral was optically uniaxial negative with indices of refraction $\omega = 1.657(3)$ and $\varepsilon = 1.621(5)$, and the empirical formula (based on 2 atoms of S apfu) $[(\text{NH}_4)_{0.73}(\text{H}_3\text{O})_{0.22}\text{K}_{0.04}\text{Na}_{0.01}]_{\Sigma 1.00}(\text{Fe}^{3+}_{0.95}\text{Al}_{0.02}\text{Mg}_{0.01})_{\Sigma 0.98}(\text{SO}_4)_2$. The single crystal X-ray diffraction study performed by Kampf et al. (2014) indicated that the Ohio sabieite crystals represent combinations of $1T$, $2H$ and $3R$ polytypes. The $1T$ polytype corresponds to the mineral from the Sabie type locality in South Africa. The other two polytypes only come from Ohio. The $2H$ polytype has a space group of $P6_3$, and unit-cell parameters of $a = 4.83380(17)$, $c = 16.4362(9)$ Å, $V = 332.59(2)$ Å³, and $Z = 2$. The $3R$ polytype belongs to a space group of $R3$ and unit-cell parameters of $a = 4.835(2)$, $c = 24.496(15)$ Å, $V = 495.9(5)$ Å³, and $Z = 3$.

Sabieite has also been determined mainly by powder X-ray diffraction (PXRD) and EMPA from the following burning coal heaps: the Anna mine, Alsdorf, Germany (Blaß and Strehler 1993), Ronneburg, Germany (Witzke and Rüger 1998), Komló and Pécs-Vasas in the Mecsek Mts., South Hungary (Szakáll and Kristály 2008), the Upper Silesian Coal Basin of Poland (Parafiniuk and Kruszewski 2009; Kruszewski 2013; Kruszewski et al. 2018), the Carola Mine, Freital, Saxony, Germany (Witzke et al. 2015) and a few other localities (some of them uncertain) reported in the Mindat Database (Mindat 2018b).

This paper provides new mineralogical data for sabieite and loncreekite and associated ferroan boussin-

gaultite and tschermigite from Libušín mine heap near Kladno, Czech Republic. A combination of methods was used to provide the reliable determination of a mixture of minerals of very similar chemical composition (sabieite, loncreekite, ferroan boussingaultite, efremitovite, tschermigite) and similar crystal structures. These included powder X-ray diffraction, electron-microprobe analysis, and Raman spectroscopy. At the same time, this study also revealed the advantages and disadvantages of the individual methods.

2. Methods

2.1. Sample

The burning waste heaps in Libušín, Kladno Coal District represent well-known localities of recently-formed, combustion-related metamorphic minerals (e.g. Rost 1937; Žáček 1988). The long-lasting burning, which possibly started shortly after the World War II, has resulted in the formation of large sulphate “caps” or “caprocks”, up to ~50 cm thick, with dominant massive Al sulphates and numerous other secondary minerals (Žáček and Povondra 1988; Jehlička et al. 2007; Žáček and Skála 2015). The most recent mineralogical studies from Libušín focussed on alunogen $\text{Al}_2(\text{SO}_4)_3 \cdot 17 \text{H}_2\text{O}$ (Košek et al. 2018a) and khademite $\text{Al}(\text{SO}_4)\text{F} \cdot 5 \text{H}_2\text{O}$ (Košek et al. 2019).

The studied sample (K302) was collected in 1987 by Vladimír Žáček on a newer waste heap (dumping started ~1940) of the former Schoeller mine¹. The sample was taken from the marginal part of the sulphate cap of the Fumarole N° 1 locality (50.1691°N, 14.0342°E; for more details see Žáček and Skála 2015), ~20 cm below the surface, where the temperature was 70–100 °C. The sample was part of a pink aggregate *c.* 15 cm across, that was relatively sharply bound from the white surroundings with a dominance of Al sulphates. The sample was stored at ambient conditions until 2017 when it was studied. The material for the instrumental study (1–3 mm grains) was separated under a binocular microscope, embedded in resin and polished by hand using a dry polishing procedure. A fraction of the hand-picked grains was used for the PXRD study.

2.2. Powder X-ray diffraction (PXRD)

Powder X-ray diffraction data were collected using the Bragg–Brentano geometry on a Bruker D8 Advance diffractometer equipped with a Lynx Eye XE detector and

¹ The Schoeller mine was established in 1899, and was renamed Nejedlý I in 1946. Since 1990, it has been again referred to as the Schoeller mine or the Kladno mine, and it closed on the 30th of June 2002.

Soller slits (2.5°) in the primary and secondary beams housed at the Czech Geological Survey in Prague. CuK_α radiation was used. The sample was gently pulverized together with acetone in an agate mortar. To minimize the background, the sample was placed on a flat silicon wafer from the acetone suspension. Diffraction data were collected in the angular range of $4\text{--}80^\circ$ of 2θ with a step of 0.015° for 0.6 s per step. An automatic divergence slit (10 mm) was employed. A qualitative phase analysis was performed using the DIFFRAC.Eva software (Bruker AXS 2015) and the PDF-2 database (ICDD 2002). The unit-cell parameters were calculated by the Rietveld method using the Topas 5 program (Bruker AXS 2014). The initial crystallographic data for tschermigite, lonecreekite, sabieite-2H, chabazite-K, anatase and quartz (i.e. the phases present in the sample) were taken from Larson and Cromer (1967), Horn et al. (1972), Le Page and Donnay (1976), Martini (1984), Kampf et al. (2014) and Lozinska et al. (2014). The refinement involved a scale factor for each phase, unit-cell parameters for each phase except quartz, sample displacement correction, and a parameter describing size broadening. The March–Dollase correction for preferred orientation in the [001] direction was applied for the sabieite. Atomic coordinates, overall isotropic displacement factors, and site occupancy parameters were fixed during the refinement for all of the phases.

2.3. Electron-microprobe analysis (EMPA)

A carbon-coated polished section of several grains was analysed using a Cameca SX-100 electron microprobe (Joint Laboratory of Masaryk University and the Czech Geological Survey in Brno, Czech Republic) operating in the wavelength-dispersion mode with an accelerating voltage of 15 kV, a sample current of 4 nA, and a beam diameter of 10 μm . K_α lines and the following standards were used: Si, Al, K – sanidine, Na – albite, Mg – Mg_2SiO_4 , Fe – almandine, Mn – spessartine, S – SrSO_4 , Ca, P – fluorapatite, F – topaz, and Cl – vanadinite. The raw data were converted to the concentrations using X- ϕ matrix correction (Merlet 1994).

Nitrogen was seen in the WDX spectra scan of both phases but not quantified. The empirical formulae of the studied minerals were calculated based on the sum of the atoms Fe + Al + Mg + Mn + S of 3, assuming stoichiometric amounts of NH_4^+ ion (and H_2O in the case of hydrated phases). The amounts of F, Cl and P_2O_5 were below the detection limit (0.15, 0.05, 0.05 wt. %, respectively) in all of the analyses.

2.4. Raman spectroscopy

Raman microspectrometric analyses of the sample were performed on a multichannel Renishaw InVia Reflex

spectrometer coupled with a Peltier-cooled CCD detector (Institute of Geochemistry, Mineralogy and Mineral Resources, Faculty of Science, Charles University in Prague). Excitation was generally provided by a 514.5 nm Ar laser (1800 lines/ mm^{-1} grating). To achieve enhanced signal-to-noise ratios, 10–25 scans were accumulated, each with a 20 s exposure time. The spectra were recorded at a spectral resolution of 2 cm^{-1} in a range of between 100 and 4000 cm^{-1} . The Benzonitrile standard was used to check the wave-number calibration. The spectra were compared using GRAMS/AI 9.1 by Thermo Fisher Scientific and not subjected to any data manipulation or processing techniques and are reported as collected, except for the baseline correction.

3. Results

The size of the sample is $9\times 7\times 7\text{ cm}$, and it is a breccia composed of angular mm–cm-sized chips of altered sedimentary rocks (mainly siltstones, partly converted to clinker) cemented by pinkish, in places whitish to yellowish material, slowly soluble in cold water (Fig. 1). The sulphate cement (crust) is 1–10 mm thick, hard, massive, slightly porous, with a fine botryoidal or irregular crystalline surface in fine cavities. Under the optical microscope and using oil immersion, the material is fine-grained with optical properties that are difficult to determine. In the back-scattered electron (BSE) images, the minerals form irregular aggregates 30–200 μm across, and intimately intergrown. The recognizable features include (1) dominant grains of mixtures of sabieite and lonecreekite and (2) minor domains of boussingaultite with traces of efremovite. Tschermigite (3) is not mixed with the other minerals, and occurs as a separate domain or veinlet $\sim 0.5\text{ mm}$ thick. Quartz and anatase are finely dispersed.

3.1. Powder X-ray diffraction (PXRD)

The PXRD study revealed prevailing lonecreekite with minor sabieite, boussingaultite, tschermigite and traces of efremovite (Fig. 2). The material also contains trace amounts of quartz and anatase. The weak diffraction at 9.45 Å corresponds well to chabazite; however, this mineral is not common in the coal-fire-related mineral paragenesis. Tobelite is not present, since this mineral would show (001) diffraction at 10.30 Å . The diffraction pattern of lonecreekite coincides largely with that of the minor tschermigite (indicated as a minor phase by EMPA). Nevertheless, the measured intensity of the (002) reflection at $14.44^\circ 2\theta$ cannot be fitted using only a lonecreekite structure in the Rietveld refinement. Adding the tschermigite structure to the refined phases improved the profile agreement factors (i.e. a decrease in R_{wp} from 18.679 to 16.493 %) and the (002) reflec-

data (see Fig. 2). The EMPA was unable to distinguish between anhydrous and hydrous minerals of the “same” composition (sabieite vs. loncreekite and efremovite vs. boussingaultite).

Loncreekite has the mean empirical formula $[(\text{NH}_4)_{0.98}\text{K}_{0.02}]_{\Sigma 1.00}(\text{Fe}_{0.70}\text{Al}_{0.24}\text{Mg}_{0.02})_{\Sigma 0.96}(\text{SO}_4)_{2.05} \cdot 12 \text{H}_2\text{O}$. By analogy, the sabieite formula is $[(\text{NH}_4)_{0.98}\text{K}_{0.02}]_{\Sigma 1.00}(\text{Fe}_{0.70}\text{Al}_{0.24}\text{Mg}_{0.02})_{\Sigma 0.96}(\text{SO}_4)_{2.05}$ (Tab. 1).

In addition to high Mg content, boussingaultite shows elevated levels of Fe and Mn, and has the following mean empirical formula: $(\text{NH}_4)_2(\text{Mg}_{0.62}\text{Fe}_{0.36}\text{Mn}_{0.06})_{\Sigma 1.04}(\text{SO}_4)_{1.97} \cdot 6 \text{H}_2\text{O}$ (Tab. 2). Tschermigite has the mean empirical formula of $[(\text{NH}_4)_{0.98}\text{K}_{0.02}]_{\Sigma 1.00}(\text{Al}_{0.97}\text{Fe}_{0.06})_{\Sigma 1.03}(\text{SO}_4)_{2.97} \cdot 12 \text{H}_2\text{O}$ (Tab. 2).

3.3. Raman spectroscopy

Based on the multiple Raman measurements of different spots, two major sulphate phases, sabieite and alum (alum means both loncreekite and tschermigite that are poorly distinguishable in the Raman spectra) were identified, along with at least two additional sulphates (boussingaultite and efremovite).

When interpreting the Raman spectra of the sulphates, the most important region is at 400–1300 cm^{-1} , where bands of the internal vibrations of sulphate ions can be observed (stretching modes ν_1 and ν_3 , and bending modes ν_2 and ν_4). Bands below 400 cm^{-1} are commonly related to cation–oxygen vibrations ($M\text{--O}$). The region between 1300 and 1800 cm^{-1} often shows bending vibrations of water and/or the ammonium group. The stretching modes of water and NH_4 molecules are typically observed at higher wavenumbers, between 2400 and 4000 cm^{-1} .

Since sabieite and alum almost always occur as intimately mixed assemblages, Raman spectra of a single phase could not be obtained despite using a focused laser beam (spot-size up to 1.5 μm at a 50 \times magnification). Figure 3 shows the two most representative shapes of the Raman spectra for the dominant phases. The first one (Fig. 3a) is dominated by two

strong bands (991 and 1037 cm^{-1}) that can be associated with the ν_1 vibration mode of the SO_4 group. The 1037 cm^{-1} band is close to the position of the ν_1 sulphate band for sabieite. Sabieite is also supported by other typical bands at 1272 cm^{-1} (ν_3), 597 and 643 cm^{-1} (ν_4), and 313 cm^{-1} (Fe–O vibration). The band at 462 cm^{-1} of the ν_2 mode is insufficiently specific in the context of the studied sample, but can probably be attributed to sabieite. The strong band at 991 cm^{-1} (ν_1), the weak band at 1132 cm^{-1} (ν_3), and the weak band at 616 cm^{-1} (ν_4) are assigned to an alum mineral.

The Raman bands of alum are better observed in the second spectrum (Fig. 3b): a strong band at 991 cm^{-1} (ν_1), a medium band at 1132 cm^{-1} and a broad band around 1104 cm^{-1} (ν_3), a medium band at 461 cm^{-1} with a weak band around 443 cm^{-1} (ν_2), and a medium band at 616 cm^{-1} with a shoulder around 634 cm^{-1} (ν_4). However, this spectrum also contains characteristic spectral signatures for sabieite at 1036 cm^{-1} (ν_1), 1271 cm^{-1} (ν_3), and 315 cm^{-1} (Fe–O).

Besides sabieite and alum, the Raman signatures of other sulphate phases were occasionally found. Figure 4 gives an example of these phases. The strong band at 982 cm^{-1} (ν_1) present in the spectrum (Fig. 4a) and

Tab. 1 Chemical composition (wt. %) of the sabieite–loncreekite mixture from Libušín (expressed as sabieite)

No	1	2	3	4	5	mean
SiO ₂	0.66	4.40	2.83	6.07	0.02	2.79
Al ₂ O ₃	7.12	5.16	5.50	5.63	3.13	5.31
Fe ₂ O ₃ (tot)	17.13	18.41	18.75	18.03	21.54	18.77
MnO	0.12	0.10	0.06	0.12	0.09	0.10
MgO	0.35	0.17	0.19	0.18	0.18	0.21
CaO	0.04	0.02	0.01	0.03	0.05	0.03
Na ₂ O	0.01	0.06	0.06	0.02	0.00	0.03
K ₂ O	0.69	0.43	0.47	0.69	0.53	0.56
SO ₃	57.37	54.30	55.17	54.78	54.72	55.27
*Al ₂ O ₃	6.85	3.31	4.31	3.08	3.12	4.13
*Fe ₂ O ₃ (tot)	17.13	18.41	18.75	18.03	21.54	18.77
*MnO	0.12	0.10	0.06	0.12	0.09	0.10
*MgO	0.35	0.17	0.19	0.18	0.18	0.21
*K ₂ O	0.61	0.00	0.13	0.00	0.53	0.25
*SO ₃	57.37	54.30	55.17	54.78	54.72	55.27
Al	0.374	0.199	0.250	0.185	0.180	0.238
Fe ³⁺	0.598	0.706	0.695	0.694	0.793	0.697
Mn	0.005	0.004	0.002	0.005	0.004	0.004
Mg	0.024	0.013	0.014	0.014	0.013	0.016
K	0.036	0.000	0.008	0.000	0.033	0.015
S	1.998	2.077	2.039	2.102	2.011	2.046
Fe/(Fe+Al)	0.615	0.780	0.735	0.789	0.815	0.747

The formulae are based on the sum of atoms Fe + Al + Mg + Mn + S = 3 and a stoichiometric amount of NH_4^+

P₂O₅, F, Cl were also analyzed but not detected

Sabieite, empirical formula No 5: $[(\text{NH}_4)_{0.97}\text{K}_{0.03}]_{\Sigma 1.00}(\text{Fe}_{0.79}\text{Al}_{0.18}\text{Mg}_{0.01})_{\Sigma 0.98}(\text{SO}_4)_{2.01}$

Sabieite, mean empirical formula: $[(\text{NH}_4)_{0.98}\text{K}_{0.02}]_{\Sigma 1.00}(\text{Fe}_{0.70}\text{Al}_{0.24}\text{Mg}_{0.02})_{\Sigma 0.96}(\text{SO}_4)_{2.05}$

*data without impurity expressed as K-chabazite: 47.62 SiO₂, 20.2 Al₂O₃, 0.16 MgO, 3.33 CaO, 0.61 Na₂O, 5.6 K₂O (WEBMINERAL 2019)

Tab. 2 Chemical composition (wt. %) of boussingaultite and tschermigite from Libušín (expressed as anhydrous phases)

No	1	2	3	mean	1	2	mean
Mineral	boussingaultite				tschermigite		
SiO ₂	13.42	7.84	12.89	11.38	0.13	0.32	0.22
Al ₂ O ₃	3.99	4.53	3.89	4.14	14.55	14.77	14.66
FeO(tot)	6.87	7.93	6.91	7.24	1.06	1.59	1.33
MnO	1.21	1.1	1.23	1.18	n.d.	n.d.	
MgO	7.67	6.88	6.6	7.05	0.03	0.06	0.05
CaO	0.13	0.13	0.28	0.18	0.11	0.12	0.11
Na ₂ O	0.07	0.09	n.d.	0.05			
K ₂ O	1.02	1.14	1.47	1.21	0.16	0.17	0.17
SO ₃	45.46	46.17	42.5	44.71	45.48	47.4	46.44
total	99.85	95.82	95.89	97.18	61.57	64.43	63.00
Al ₂ O ₃					14.5	14.6	14.55
FeO(tot)	6.87	7.93	6.91	7.24	1.06	1.59	1.33
MnO	1.21	1.1	1.23	1.18			
MgO	7.67	6.88	6.6	7.05			
K ₂ O					0.16	0.17	0.17
SO ₃	45.46	46.17	42.5	44.71	45.48	47.4	46.44
Al					0.984	0.954	0.969
Fe ²⁺	0.330	0.379	0.357	0.355	0.051	0.074	0.062
Mn	0.059	0.053	0.064	0.059			
Mg	0.655	0.586	0.608	0.617			
K					0.012	0.012	0.012
S	1.957	1.981	1.97	1.969	1.965	1.972	1.968
total	3.001	2.999	3.000	3.000	3.011	3.012	3.012
XMg	0.628	0.576	0.591	0.598			
XFe	0.316	0.372	0.347	0.345			
XMn	0.056	0.052	0.062	0.057			

The formulae are based on the sum of atoms Fe + Al + Mg + Mn + S = 3, assuming a stoichiometric amounts of NH⁴⁺ and H₂O. The Si, Al, Ca, Na and K in boussingaultite are considered as impurities. P₂O₅, F, Cl were also analyzed but not detected, n.d. – not detected

Boussingaultite mean empirical formula: (NH₄)_{4/2}(Mg_{0.62}Fe_{0.36}Mn_{0.06})_{1.04}(SO₄)_{1.97}·6H₂O

Tschermigite mean empirical formula: [(NH₄)_{0.98}K_{0.02}]_{1.00}(Al_{0.97}Fe_{0.06})_{1.03}(SO₄)_{1.97}·12H₂O

coupled with the shoulder at 450 cm⁻¹ (ν₂) and the band at 625 (ν₄) cm⁻¹ both strongly suggest boussingaultite (Culka et al. 2009). Other bands can be attributed to sabieite or alum. A very weak signature of efremovite can be found in another spectrum (Fig. 4b) around 1052 cm⁻¹, but no other observable bands can be easily associated with this band (Košek et al. 2018b). Instead, they are assigned to alum and sabieite.

All of the identified sulphate phases contain an ammonium cation. Alum and boussingaultite also feature water molecules. Due to the complexity of the investigated sample, bands associated with the bending vibrations of ammonium or water molecules in the 1300–1800 cm⁻¹ spectral region are not specific for any of the identified phases. Nevertheless, these bands can serve as auxiliary data confirming the presence of the ammonium group or water in the investigated minerals. Bands of the ν₄ bending vibrations of the NH₄ group between 1420 and 1440 cm⁻¹ were found in all the spectra. Bands of the ν₂ bending vibrations of the NH₄ group overlap with H₂O

vibrations around 1600 cm⁻¹. The width and the relative intensity of these bands increase when H₂O-bearing phases are present. The second-order region (around 2600–4000 cm⁻¹) is shown for alum with subordinate sabieite in Fig. 3c. A large multicomponent broad band with two observable maxima is the only spectral feature in this region. It consists of overlapping bands belonging to stretch modes of water and ammonium cations, but these bands cannot be assigned to a specific sulphate phase. The approximate band positions are summarized in Tab. 3.

The Raman data of the studied sabieite are in good agreement with those previously reported for a synthetic phase (Košek et al. 2018b) and another natural sample from Ostrava, Czech Republic (Košek et al. 2017). The band positions of the minor phases also correspond to the efremovite and boussingaultite reported by Košek et al. (2017) and Culka et al. (2014), respectively.

In the case of alum, distinguishing between members of the alum group is sometimes problematic and depends on very small differences in spectral shapes and minor shifts of several bands. The identified alum has a similar shape to those of tschermigite or loncreekite reported by Frost and Klopogge (2001) and Culka et al. (2014), respectively. Some specific and relatively intense bands, probably associated with the Fe–O vibrations or Fe-related vibrations, are lacking in the obtained Raman spectra for the alum phase. This usually favours tschermigite over loncreekite (Tab. 3), but it should also be considered that this alum phase occurs strictly with sabieite, and thus this alum is formed by the hydration of sabieite. The missing or low-intensity bands can be linked to the high aluminium content of loncreekite. The spectroscopic study of synthetic alums revealed that both Al- and Fe-alum produce a Raman band associated with the ν₁ (MO₆) mode (typically observed between 290 and 340 cm⁻¹) at different positions and with different intensities (Tregenna-Piggott and Best 1996). Generally, when Fe is substituted for Al, this band shifts to higher wavenumbers (from 307 to 329 cm⁻¹ for

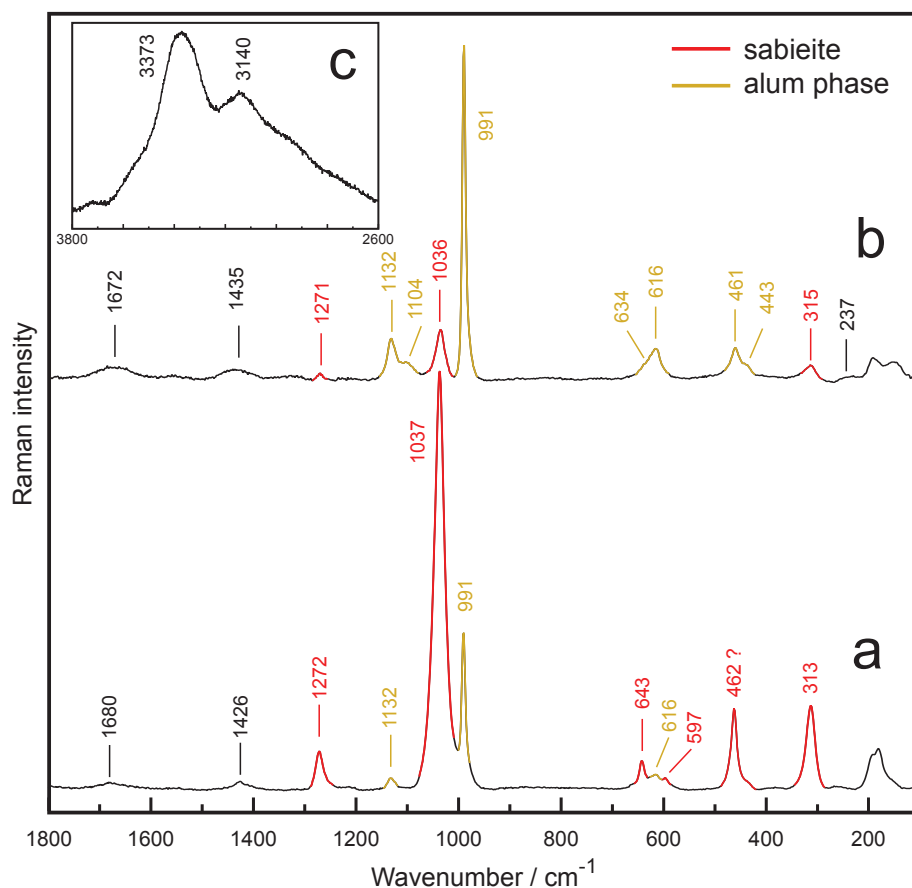


Fig. 3 Raman spectra of the sabieite (a) and an alum phase (b) displayed in the 100–1800 cm^{-1} spectral region. The second order spectra (2600–3800 cm^{-1}) are also displayed for the spot dominated by the alum phase (c).

natural specimens) and the intensity decreases (Frost and Kloprogge 2001; Culka et al. 2014). Therefore, partial substitution may explain the relatively low intensity and shift of this band. However, the Raman signal of this vibrational mode in the studied sample that is found at *c.* 313–315 cm^{-1} is probably masked with, or influenced by, a relatively strong signal of Fe–O vibrations assigned to sabieite at 315 cm^{-1} . Therefore, the band observed in the spectra cannot be entirely connected with the $\nu_1(MO_6)$ mode of the alum.

4. Discussion

The ammonium-bearing ferric sulphates loncreekite $(\text{NH}_4)\text{Fe}^{3+}(\text{SO}_4)_2 \cdot 12 \text{H}_2\text{O}$, and sabieite $(\text{NH}_4)\text{Fe}^{3+}(\text{SO}_4)_2$, with subordinated boussingaultite, tschermigite, and traces of efremovite, quartz, anatase and probable chabazite-K originated as rare products of a subsurface combustion of a waste pile in Libušín, Kladno coal district. The locality is well-known for abundant occurrences of a variety of ammonium-bearing sulphates: ammonioalunite $\text{NH}_4\text{Al}_3(\text{SO}_4)_2(\text{OH})_6$, boussingaultite $(\text{NH}_4)_2\text{Mg}(\text{SO}_4)_2 \cdot 6 \text{H}_2\text{O}$, efremovite $(\text{NH}_4)_2\text{Mg}_2(\text{SO}_4)_3$, godovikovite $\text{NH}_4\text{Al}(\text{SO}_4)_2$, letovicite $(\text{NH}_4)_3\text{H}(\text{SO}_4)_2$, mascagnite $(\text{NH}_4)_2(\text{SO}_4)$, tschermigite $(\text{NH}_4)_4\text{Al}(\text{SO}_4)_2 \cdot 12 \text{H}_2\text{O}$, and unnamed $(\text{NH}_4)_4\text{Al}(\text{SO}_4)_2 \cdot 4\text{H}_2\text{O}$, along with

some 50 other species of recently formed secondary minerals (Žáček and Skála 2015). A combination of analytical methods including PXRD, EMPA and Raman spectroscopy were applied in order to determine reliably all the minerals present in the studied sample. The complexity of the sample phases is notable. On the one hand, the sample contains a mixture of anhydrous phases and their hydrated derivatives that have the same stoichiometry (loncreekite *vs.* sabieite, see also Culka et al. 2009 or Košek et al. 2018b). On the other hand, in the sample occur iso-structural minerals with different chemical compositions (loncreekite *vs.* tschermigite). Minor efremovite was not reliably detected by PXRD, due to considerable overlapping of its PXRD pattern with those of predominant boussingaultite and tschermigite. However, it was safely revealed by Raman spectroscopy.

Aluminium-bearing sulphates – alunogen, millosevichite, tschermigite and godovikovite – strongly predominate over their ferric and ferroan analogues (Stracher et al. 2015). This results from the composition of primarily Al-rich and Fe-poor siliciclastic rocks (claystones, siltstones, sandstones, arkoses, conglomerates) and coal itself. These petrochemical peculiarities are also typical of the Kladno coal district, where the aluminium-bearing sulphates mentioned above also commonly dominate in the sulphate crusts (see Žáček and Skála 2015).

Tab. 3 Raman bands and band assignments of four measured spots in sample K302 from Libušín.

(Fig. 3a)	K302 (selected spectra)		syn. sabiete	sabiete	loncreekite	tschermigite	boussingaultite	Assignments
(Fig. 3b-c)	(Fig. 4a)	(Fig. 4b)	(Košek et al. 2018)	(Košek et al. 2017)	(Frost and Klopogge 2001)	(Culka et al. 2014)	(Culka et al. 2009)	
151 w	158 w	155 w						lattice vibration
182 m	182 m	181 m						lattice vibration
193 m	193 m	193 m	183 m					lattice vibration
237 vw br								lattice vibration
313 s (S)	313 s (S)	330 w	315 s	315 s	307	329 w	310	lattice vibration
443 w (A)		442 sh (A)		435		441 mw		lattice vibration
462 s (S?)	461 m (A)	462 s (S?)	462 s	464 m	463	459 m	454	v ₂ (SO ₄)
597 vw (S)		450 sh (B)			525			v ₂ (SO ₄)
616 vw (A)	616 m (A)	615 sh	593 w	603 m	615	615 m	616	v ₂ (SO ₄)
634 sh (A)	634 sh (A)	625 m (B)				630 sh	626	v ₂ (SO ₄)
643 w (S)	642 w (S)	642 w (S)	641 w	646 m	636	981 sh		v ₂ (SO ₄)
991 s (A)	991 vs (A)	982 vs (B)			701		983	v ₁ (SO ₄)
1037 vs (S)	1036 m (S)	1037 vs (S)			991	991 vs		v ₁ (SO ₄)
	1104 w (A)	990 vs (A)						v ₁ (SO ₄)
		1034 w (S?)	1035 vs	1041 vs				v ₁ (SO ₄)
		1052 w (E?)						v ₁ (SO ₄)
		~1102 br (A)			1099		1063	v ₃ (SO ₄)
1132 w (A)	1132 m (A)	1131 vw			1108	1102 br	1096	v ₃ (SO ₄)
1272 m (S)	1271 vw (S)	1271 m (S)				1123 sh		v ₃ (SO ₄)
		1333 br				1131 m	1133	v ₃ (SO ₄)
		1331 br						v ₃ (SO ₄)
1426 br	1435 w br	1431 br	1428 w			1442 w	1436	v ₄ (NH ₄)
		1602 br	1458 w				1460	v ₄ (NH ₄)
1680 br	1672 w br	1682 br	1681 w			1620 vw,br	1678	v ₂ (NH ₄) or v ₂ (H ₂ O)
			1714 w			1680 vw,br	1705	v ₂ (NH ₄) or v ₂ (H ₂ O)
	3140 br							(NH ₄) or (H ₂ O) vib.
	3373 br							(NH ₄) or (H ₂ O) vib

S – sabiete, A – alum phase (tschermigite or loncreekite), B – boussingaultite, E – efremovite.

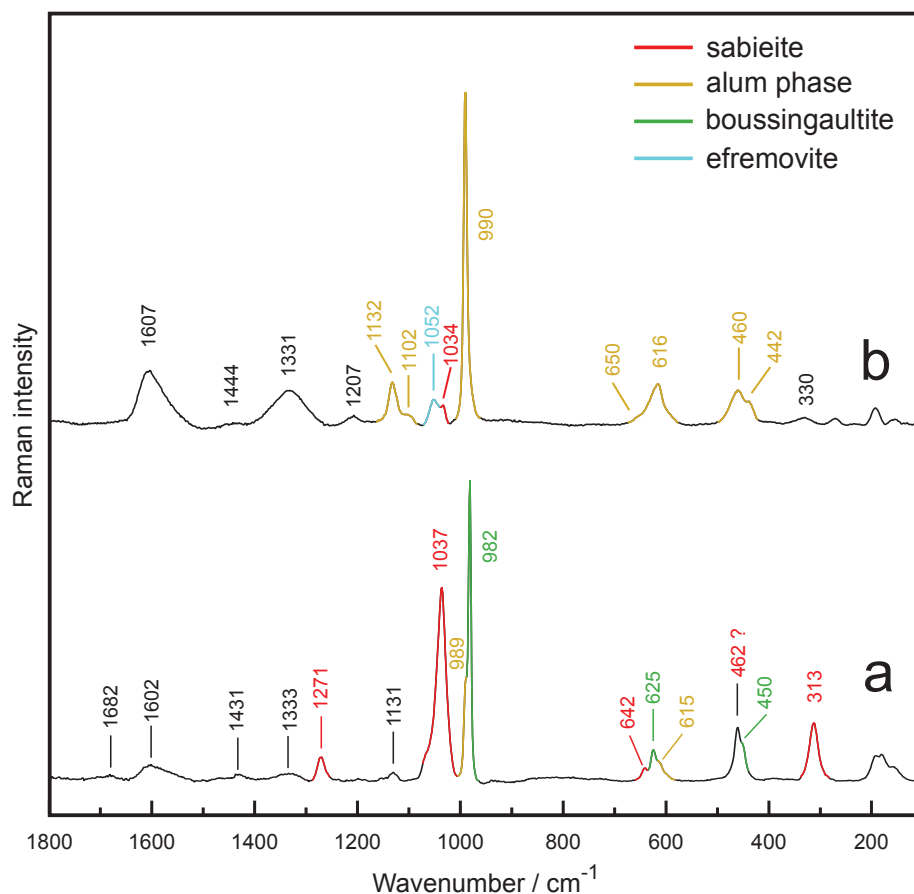


Fig. 4 Raman spectra illustrating minor phases in the sample K302 displayed in the 100–1800 cm^{-1} spectral region – dominant alum with low intensity Raman signatures of efremovite and sabieite (a) as well as sabieite with boussingaultite (b).

In contrast to abundant Al-sulphates, ferric ammonium sulphate is very rare. The sample was part of an approximately 15-cm large pink aggregate that was sharply separated from the surroundings with the dominance of Al sulphates. This type of occurrence is indicative of an *in-situ* formation by reaction of aggressive gases with a material rich in Fe (probably siderite), although the minerals can also originate by direct crystallization from the gas or as pre-crystal nuclei from the gas phase (e.g. Kruszewski et al. 2018). The reaction of $(\text{NH}_4)_3\text{H}(\text{SO}_4)_2$ with silicic rocks was described by e.g. Stoch et al. (1980). Siltstones with siderite admixtures and pelosiderite concretions are frequently found near coal seams and therefore occur in the heap material (Žáček 1995). The dominant Fe and elevated Mg and, especially, Mn contents in the sulphates are consistent with the compositions of siderite, which is a main carrier of manganese and contains 0.2–2.9 (median 1.0) wt. % MnO (based on a set of 40 unpublished siderite analyses of the authors). The K, Si, Al come from omnipresent primary illite (Žáček 1995). Ammonium is a product of thermal decomposition of organic matter, and the sulphur is mainly bound to the pyrite abundant in coal and present as organic S in the coal itself. Moreover, the presence of ammonium-bearing compounds was also confirmed by nucleation of solid ammonium-bearing minerals: letovicite, $(\text{NH}_4)_3\text{H}(\text{SO}_4)_2$, mascagnite, $(\text{NH}_4)_2(\text{SO}_4)$

and sal ammoniac, NH_4Cl (Žáček and Skála 2015). The minerals most probably originated as anhydrous phases at $\sim 115\text{--}350^\circ\text{C}$. The lower temperature limit of 115°C is supported by the transition of hydrated boussingaultite to anhydrous efremovite (Fellner and Khandl 2004). The ammonium sulphate godovikovite, $\text{NH}_4\text{Al}(\text{SO}_4)_2$, isostructural with sabieite $(\text{NH}_4\text{Fe}^{3+}(\text{SO}_4)_2)$, has the upper limit of thermal stability at $\sim 400^\circ\text{C}$ (Žáček 1988). However, the maximum temperature (350°C) measured at the studied locality by Žáček (1988) is considered as the upper limit. After being stored under ambient conditions for 30 years, the relatively high-temperature anhydrous sabieite and efremovite, which were primarily formed in a fumarole environment, have been slowly hydrated and converted into loncreekite and boussingaultite, respectively.

5. Conclusions

This paper provides new mineralogical data – Powder X-ray diffraction (PXRD), unit-cell parameters, chemical compositions and Raman spectra of sabieite and loncreekite and the associated ferroan boussingaultite with tschermigite from Libušín near Kladno, Czech Republic.

The studied sample consists of a fine-grained mixture of both anhydrous and hydrous ammonium-bearing Fe,

Al, Mg sulphates. The presence of isostructural phases (in this case loncreekite and tschermigite) makes conventional PXRD phase analysis difficult or nearly impossible. On the other hand, the PXRD identified safely several mineral species: dominant alum, minor sabieite, and subordinate boussingaultite, efremovite, as well as traces of chabazite-K, anatase, and quartz.

The EMPA discovered three homogeneous chemical compounds: ammonium iron sulphate (attributed to a fine-grained mixture of dominant loncreekite and minor sabieite), ammonium magnesium sulphate (attributed to boussingaultite with traces of efremovite) and hydrous ammonium aluminium sulphate (attributed to tschermigite). The tschermigite was not safely identified by the PXRD due to an overlap in the diffraction pattern with loncreekite. The excess of K, Si and Al found repeatedly in the EMPA data was attributed to finely dispersed chabazite-K, also detected by PXRD.

The Raman analyses confirmed the presence of at least four phases: dominant alum (loncreekite and/or tschermigite, which were poorly distinguishable in the Raman spectra) and minor sabieite, boussingaultite and efremovite.

The empirical formula of loncreekite is $[(\text{NH}_4)_{0.98}\text{K}_{0.02}]_{\Sigma 1.00}(\text{Fe}_{0.70}\text{Al}_{0.24}\text{Mg}_{0.02})_{\Sigma 0.96}(\text{SO}_4)_{2.05} \cdot 12 \text{H}_2\text{O}$, and the calculated unit-cell ($P\bar{a}3$) parameter is $a = 12.2442(2) \text{ \AA}$, with a cell volume of $V = 1835.68(9) \text{ \AA}^3$.

The composition of sabieite corresponds to $[(\text{NH}_4)_{0.98}\text{K}_{0.02}]_{\Sigma 1.00}(\text{Fe}_{0.70}\text{Al}_{0.24}\text{Mg}_{0.02})_{\Sigma 0.96}(\text{SO}_4)_{2.05}$, and the calculated unit-cell parameters ($P3_21$) are: $a = 4.826(1) \text{ \AA}$, $c = 8.283(2) \text{ \AA}$, $V = 167.10(8) \text{ \AA}^3$, assuming that only the 1T polytype is present. Raman spectroscopy for sabieite gives strong bands at 1037 cm^{-1} (ν_1), 1272 cm^{-1} (ν_3), 462 cm^{-1} (ν_2), 643 cm^{-1} (ν_4), and 313 cm^{-1} ($M-O$ vibration). For loncreekite it gives bands at 991 cm^{-1} (ν_1), 1132 and 1104 cm^{-1} (ν_3), 461 and 443 cm^{-1} (ν_2), and 616 cm^{-1} (ν_4) (where ν_1 and ν_3 are stretching modes of the (SO_4) -group and ν_2 and ν_4 are bending modes).

Boussingaultite has the mean empirical formula $(\text{NH}_4)_2(\text{Mg}_{0.62}\text{Fe}_{0.36}\text{Mn}_{0.06})_{\Sigma 1.04}(\text{SO}_4)_{1.97} \cdot 6 \text{H}_2\text{O}$ and tschermigite $[(\text{NH}_4)_{0.98}\text{K}_{0.02}]_{\Sigma 1.00}(\text{Al}_{0.97}\text{Fe}_{0.06})_{\Sigma 1.03}(\text{SO}_4)_{2.97} \cdot 12 \text{H}_2\text{O}$.

This study illustrates that a combination of several analytical methods is required for reliable mineralogical identification of complex mixtures containing sulphate minerals of various degrees of hydration. It also reveals the advantages and limitations of the individual methods.

Acknowledgements. This study was financed by the Czech Science Foundation grant project “A model of mobilization and geochemical cycles of potentially hazardous elements and organic compounds in burnt coal heaps” (GACR 15-11674S panel P210) and by the research project of the Czech Geological Survey No. 321 183. It was also supported by grant No. 338 415 from the Grant

Agency of Charles University. The authors are grateful to Ella Sokol and Łukasz Kruszewski for valuable reviews, Jiří Sejkora and Vojtěch Janoušek for careful handling and the comments and to the anonymous proof-reader for improvement of the English language.

References

- BLASS G, STREHLER H (1993) Mineralbildungen in einer durch Selbstentzündung brennenden Bergehalde des Aachener Steinkohlenreviers. *Miner Welt* 4: 35–42
- BRUKER AXS (2014) Topas Program, ver. 5. Karlsruhe, Germany
- BRUKER AXS (2015) DIFFRAC_EVA Program, ver. 4.1. Karlsruhe, Germany
- CARLSON E (2010) Analysis of Huron River shale fire minerals reveals two specimens new to Ohio. *Ohio Geol* 2: 7
- CULKA A, JEHLIČKA J, NĚMEC I (2009) Raman and infrared spectroscopic study of boussingaultite and nickelboussingaultite. *Spectrochim Acta A, Mol Biomol Spectrosc* 73: 420–423
- CULKA A, KOŠEK F, DRAHOTA P, JEHLIČKA J (2014) Use of miniaturized Raman spectrometer for detection of sulphates of different hydration states – significance for Mars studies. *Icarus* 243: 440–453
- CRYSTAL MAKER SOFTWARE LTD. (2018) Crystal Diffract Program, ver. 6.7.4. Begbroke, Oxfordshire, UK
- FELLNER P, KHANDEL V (2004) Phase diagram of the reciprocal system 2NH_4^+ , $\text{Mg}^{2+}/(\text{SO}_4)^{2-}$, $2(\text{NO}_3)^-$ – H_2O . *Chem Pap* 58: 221–223
- FROST L, KLOPROGGE JT (2001) Raman microscopic study of kalinite, tschermigite and loncreekite at 297 and 77 K. *Neu Jb Mineral, Mh* 1: 27–40.
- GENDRIN A, MANGOLD N, BIBRING JP, LANGEVIN Y, GONDET B, POULET F, BONELLO G, QUANTIN C, MUSTARD J, ARVIDSON R, LEMOUÉLIC S (2005) Sulfates in Martian layered terrains: the OMEGA/Mars Express view. *Science* 307: 1587–1591
- HORN M, SCHWERDTFEGER CF, MEAGHER EP (1972) Refinement of the structure of anatase at several temperatures. *Z Kristallog Krist* 136: 273–281
- ICDD (2002) In: McCLUNE F (ed) PDF-2 Powder Diffraction File. International Centre for Diffraction Data (ICDD), 12 Campus Boulevard, Newton Square, Pennsylvania, 19073-3272
- JEHLIČKA J, ŽÁČEK V, EDWARDS HGM, SHCHERBAKOVA E, MOROZ N (2007) Raman spectra of organic compounds kladnoite ($\text{C}_6\text{H}_4(\text{CO})_2\text{NH}$) and hoelite ($\text{C}_{14}\text{H}_8\text{O}_2$) – rare sublimation products crystallizing on self-ignited coal heaps. *Spectrochim Acta A, Mol Biomol Spectrosc* 68: 1053–1057
- KAMPF A, RICHARDS R, NASH B (2014) The 2H and 3R polytypes of sabieite, $\text{NH}_4\text{Fe}^{3+}(\text{SO}_4)_2$, from a natural fire

- in an oil-bearing shale near Milan, Ohio. *Amer Miner* 99: 1500–1506
- KOŠEK F, CULKA A, JEHLIČKA J (2017) Field identification of minerals at burning coal dumps using miniature Raman spectrometers. *J Raman Spectrosc* 48: 1494–1502
- KOŠEK F, CULKA A, ŽÁČEK V, LAUFEK F, ŠKODA R, JEHLIČKA J (2018a) Native alunogen: a Raman spectroscopic study of a well-described specimen. *J Mol Struct* 1153: 191–200
- KOŠEK F, CULKA A, JEHLIČKA J (2018b) Raman spectroscopic study of six synthetic anhydrous sulphates relevant to the mineralogy of fumaroles. *J Raman Spectrosc* 49: 1205–1216
- KOŠEK F, ŽÁČEK V, ŠKODA R, LAUFEK F, JEHLIČKA J (2019) New mineralogical data for khademite (orthorhombic $\text{AlSO}_4 \cdot 5 \text{H}_2\text{O}$) and the story of rostitite (orthorhombic $\text{AlSO}_4 \cdot \text{OH} \cdot 5 \text{H}_2\text{O}$) from Libušín near Kladno, the Czech Republic. *J Mol Struct* 1175: 208–213
- KRUSZEWSKI Ł (2013) Supergene sulphate minerals from the burning coal mining dumps in the Upper Silesian Coal Basin, South Poland. *Int J Coal Geol* 105: 91–109
- KRUSZEWSKI Ł, FABIAŃSKA MJ, CIESIELCZUK J, SEGIT T, ORŁOWSKI R, MOTYLIŃSKI R, MOSZUMAŃSKA I, KUSY D (2018) First multi-tool exploration of a gas-condensate–pyrolysate system from the environment of burning coal mine heaps: an in situ FTIR and laboratory GC and PXRD study based on Upper Silesian materials. *Sci Total Environ* 640–641: 1044–1071
- LARSON AC, CROMER DT (1967) Refinement of the alum structures. III. X-ray study of the alpha-alums, K, Rb and $\text{NH}_4\text{Al}(\text{SO}_4)_2 \cdot (\text{H}_2\text{O})_{12}$. *Acta Crystallogr* 22: 793–800
- LE PAGE Y, DONNAY G (1976) Refinement of the crystal structure of low-quartz. *Acta Cryst B* 32: 2456–2459
- LOZINSKA MM, MOWAT JPS, WRIGHT PA, THOMPSON SP, JORDA JL, PALOMINO M, VALENCIA S, REY F (2014) Cation gating and relocation during the highly selective “trapdoor” adsorption of CO_2 on univalent cation forms of zeolite Rho. *Chem Mater* 26: 2052–2061
- MARTINI JEJ (1984) Lonecreekite, sabieite, and clairite, new secondary ammonium ferric-iron sulphates from Lone Creek Fall cave, near Sabie, eastern Transvaal. *Ann Geol Surv (South Africa)* 17: 29–34
- MERLET C (1994) An accurate computer correction program for quantitative electron probe microanalysis. *Microchim Acta* 114/115: 363–376
- MINDAT (2018a) Lonecreekite. Accessed on January 30, 2018 at <https://www.mindat.org/min-2430.html>
- MINDAT (2018b) Sabieite. Accessed on January 30, 2018 at <https://www.mindat.org/min-3494.html>
- MINDAT (2019) Lonecreekite. Accessed on May 21, 2019 at <https://www.mindat.org/locentry-894338.html>
- PARAFINIUK J, KRUSZEWSKI Ł (2009) Ammonium minerals from burning coal-dumps of the Upper Silesian Coal Basin (Poland). *Geol Q* 53: 341–356
- ROST R (1937) The minerals formed on burning heaps in the coal basin of Kladno. *Rozpr Čs Akad Věd, Ř mat příř Věd* 47: 1–7
- STOCH L, SIKORA WS, BUDEK L (1980) A study of reactions of layer silicates with molten ammonium sulphate – part I. Reactions of kaolinite, halloysite, muscovite and biotite with $(\text{NH}_4)_2\text{SO}_4$ at 350 °C. *Miner Polon* 11: 61–79
- STOIBER RE, ROSE WI (1974) Fumarole incrustation at active Central American volcanoes. *Geochim Cosmochim Acta* 38: 495–516
- STRACHER GB, PRAKASH A, SOKOL EV (2015) Coal and Peat Fires: A Global Perspective, Volume 3: Case Studies – Coal Fires. Elsevier, Amsterdam, pp 1–786
- SZAKÁLL S, KRISTÁLY F (2008) Ammonium sulphates from burning coal dumps at Komló and Pécs-Vasas, Mecsek Mts., South Hungary. *Mineralogia, Spec Pap* 32: 154
- TREGENNA-PIGGOTT PLW, BEST SP (1996) Single-crystal Raman spectroscopy of the rubidium alums $\text{RbM}^{\text{III}}(\text{SO}_4)_2 \cdot 12 \text{H}_2\text{O}$ ($\text{M}^{\text{III}} = \text{Al, Ga, In, Ti, V, Cr, Fe}$) between 275 and 1200 cm^{-1} : correlation between the electronic structure of the trivalent cation and structural abnormalities. *Inorg Chem* 35: 5730–5736
- WEBMINERAL (2019) Chabazite-K. Accessed on May 21 2019, at <http://webmineral.com/data/Chabazite-K.shtml#XOOt1di3xaT>
- WITZKE T, RÜGER F (1998) Die Minerale der Ronneburger und Culmischer Lagerstätten in Thüringen. *Lapis* 23: 26–64
- WITZKE T, DE WIT F, KOLITSCH U, BLASS G (2015) Mineralogy of the burning Anna I coal mine dump, Alsdorf, Germany. In: STRACHER GB, PRAKASH A, SOKOL EV (2015) Coal and Peat Fires: A Global Perspective, Volume 3: Case Studies – Coal Fires. Elsevier, Amsterdam, pp 203–240
- ŽÁČEK V (1988) Zonal association of secondary minerals from burning dumps of coal mines near Kladno, Central Bohemia, Czechoslovakia. *Acta Univ Carol, Geol* 3: 315–341
- ŽÁČEK (1995) Inclusions of soluble chlorides in the pelosiderite groundmass from the Kladno coal district, Czech Republic. *Bul mineral-petrolog Odd Nár Muz (Praha)* 3: 231 (in Czech)
- ŽÁČEK V, POVONDRA P (1988) New mineralogical data for rostitite from Libušín, Central Bohemia, Czechoslovakia. *Neu Jb Mineral, Mh* 10: 476–480
- ŽÁČEK V, SKÁLA R (2015) Mineralogy of burning-coal waste piles in collieries of the Czech Republic. In: STRACHER GB, PRAKASH A, SOKOL EV (2015) Coal and Peat Fires: A Global Perspective, Volume 3: Case Studies – Coal Fires. Elsevier, Amsterdam, pp 109–159